Electron phase and spin decoherence in the vicinity of the second subband edge in an asymmetrical quantum well

2004 J. Phys.: Condens. Matter 16 641

(http://iopscience.iop.org/0953-8984/16/4/013)

INSTITUTE OF PHYSICS PUBLISHING JOURNAL OF PHYSICS: CONDENSED MATTER

J. Phys.: Condens. Matter **16** (2004) 641–650 PII: S0953-8984(04)69537-3

Electron phase and spin decoherence in the vicinity of the second subband edge in an asymmetrical quantum well

I G Saveliev[1,2], D D Bykanov[1], S V Novikov[1,3], T A Polyanskaya[1] and H Ruda[2]

[1] Ioffe Institute, Russian Academy of Sciences, 194021 St Petersburg, Russia
[2] University of Toronto, 170 College St, Toronto, ON, M5S 3E3, Canada
[3] University of Nottingham, School of Physics and Astronomy, Nottingham NG7 2RD, UK

Received 26 September 2003
Published 16 January 2004
Online at stacks.iop.org/JPhysCM/16/641 (DOI: 10.1088/0953-8984/16/4/013)

Abstract

Weak antilocalization of a two-dimensional electron gas formed at a $In_{0.53}Ga_{0.47}As$/InP heterointerface was studied. The Fermi level was varied from below, to above, the energy minimum of the second subband. A model for quantum coherence with two conducting subbands and fast intersubband scattering was used to extract the characteristic phase and spin decoherence rates from experimental magnetoresistance data. Taking into account the spatial inhomogeneity of the energy associated with the subband minimum, the first and second subband decoherence contributions were separated. It was shown that phase decoherence in the second subband is much faster than in the first subband and it decreases with increasing occupation of the second subband. By contrast, spin dephasing due to scattering in the second subband and intersubband scattering does not play a noticeable role.

Spin coherence is a key requirement for future semiconductor-based spintronic devices [1] and quantum computers [2]. Spin–orbit interactions determine the spin coherence time of electrons in such semiconductor structures. Recent theoretical studies [3] reveal a complex picture for spin–orbit splitting of the two-dimensional (2D) electron subbands, determined by intrinsic and artificial asymmetries of these structures. It was shown that these effects are not additive [4] and provide anisotropy in the characteristic times [5]. While these characteristics underline the importance of experimental studies of spin–orbit subband splitting in semiconductor nanostructures, they also make such experiments challenging.

One of the most powerful methods for studying spin–orbit splitting in semiconductor quantum wells is investigating low temperature quantum coherent transport [6, 7]. For fast spin–orbit (SO) relaxation $\tau_s \leqslant \tau_\varphi$ [8], where τ_s and τ_φ are the SO and phase relaxation times, respectively. Spin splitting of the energy states determines the rate of

Table 1. Low temperature (1.8 K) 2DEG parameters for two typical samples of LPE grown selectively doped $In_{0.53}Ga_{0.47}As/InP$ heterostructures.

	Initial state		First subband parameters					
Sample No	n_s (10^{11} cm^{-2})	μ (10^4 cm^2 V^{-1} s^{-1})	τ (ps)	τ_φ (ps)	τ_s (ps)	τ_{12}^* (ps)	E_2 (meV)	Γ_2 (meV)
1	2.9	3.82	1.03	20.5	5.23	2.3 ± 0.5	10.05 ± 0.03	0.38 ± 0.02
2	4.2	2.52	0.74	35.7	2.63	4.5 ± 0.7	14.3 ± 0.05	0.27 ± 0.02

spin–orbit scattering and its density dependence. Fast SO relaxation leads to a positive magnetoresistance at low magnetic fields, which changes to negative magnetoresistance at higher fields. Therefore, a so-called antilocalization maximum in the magnetoresistance or a minimum in the magnetoconductivity with increasing magnetic fields was predicted [9].

For a 2D electron gas (2DEG) an antilocalization maximum in the magnetoresistance was experimentally observed in GaAs-based heterostructures [6, 10] but subsequent experiments demonstrated that the influence of the SO scattering is much more pronounced in $In_{0.53}Ga_{0.47}As/InP$ heterostructures [7, 11]. These latter studies on asymmetric quantum wells in $In_{0.53}Ga_{0.47}As/InP$ heterostructures enabled the main physical mechanisms for SO relaxation in the 2DEG to be studied [7, 11, 12]. The goal of this paper is to clarify the contribution of electrons in the second subband to the spin and phase decoherence of electrons in an asymmetric quantum well.

Analysis of the theory [13] shows that the most direct way to experimentally determine the electron coherence time in the second subband is to study weak localization in a sample, preferably having short range scatterers. In this case, intersubband scattering can be sufficiently fast to yield averaged characteristics of the 2DEG filling two subbands. Normally at low temperatures, the main mechanism limiting the mobility of such a 2DEG is ionized impurity scattering [14], which is long range. Hence, for our experiments we choose selectively doped $In_{0.53}Ga_{0.47}As/InP$ heterostructures grown by liquid phase epitaxy (LPE) on semi-insulating InP substrates [15]. Both the InP buffer layer and the $In_{0.53}Ga_{0.47}As$ layers were grown using Sm as the getter impurity in the liquid phase. This provides very lightly doped layers with p-type conductivity [16]. The 2DEG is localized in the $In_{0.53}Ga_{0.47}As$ layer in the asymmetrical potential well near the $In_{0.53}Ga_{0.47}As/InP$ heterointerface. We choose samples with 2DEG densities in the range (3–5) $\times$ 10^{11} cm^{-2} providing only first subband occupation in the initial equilibrium state and occupation of the second subband in the saturated persistent photoconductivity state. Parameters for two typical samples are given in table 1. Comprehensive investigations of the carrier density dependence of the 2DEG mobility $\mu(n_s)$ in the $In_{0.53}Ga_{0.47}As/InP$ structures at liquid helium temperatures [17, 18] demonstrated that for $n_s > 2 \times 10^{11}$ cm^{-2} the main scattering mechanism is alloy disorder scattering [19] limiting the mobility to (1–2) $\times$ 10^5 cm^2 V^{-1} s^{-1} and interface roughness scattering [20]. LPE cannot provide an ultrasmooth heterointerface. The roughness parameters were an rms amplitude of 0.7 nm and a period of 5 nm [18]. For our investigations it is important that alloy disorder and spatial interface fluctuations are both described by a short range scattering potential.

Experiments were performed at 1.8 K. A DC measurement system was used for measuring the Hall effect and weak anomalous magnetoresistance at low magnetic fields $|B| < 100$ G. The 2DEG density was varied using the persistent photoconductivity effect induced by light pulses from a GaAs light-emitting diode placed on the sample holder. Persistent photoconductivity originates from the spatial separation of photoinduced carriers by the internal electric field. As a result, electrons are trapped in the potential well and increase the 2DEG density while

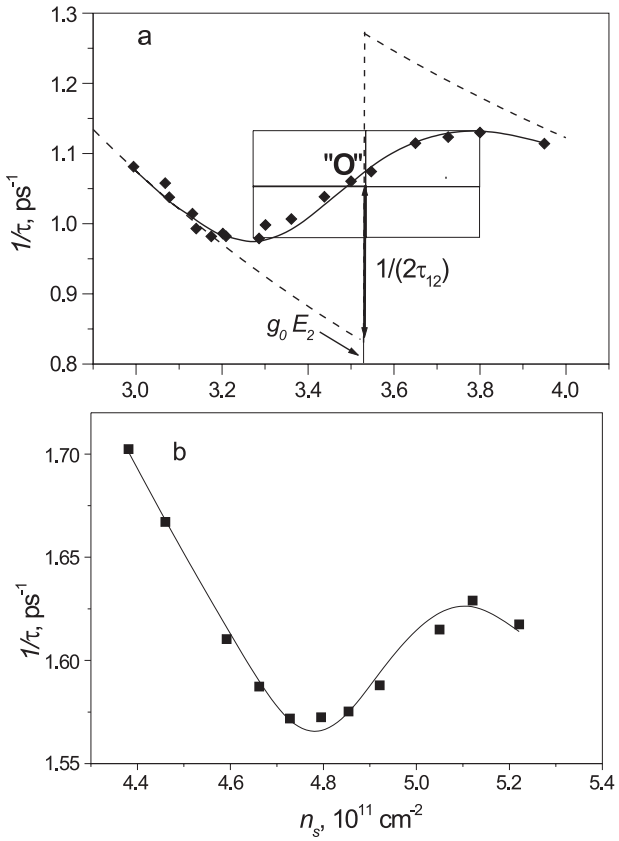

Figure 1. The dependence of the transport relaxation rate on the Hall density of a two-dimensional electron gas at the $In_{0.53}Ga_{0.47}As$/InP heterointerface in sample No 1 (a) and No 2 (b). Points are experimental data corresponding to a series of sample states after illumination pulses at 1.8 K. The transport relaxation rate increase is attributed to the contribution of intersubband scattering once the second subband starts to be populated. Dotted curves are calculated for an ideal step-like density of states. Solid curves are the result of fitting using equations (3) and (4) and taking into account the density of states originating from spatial inhomogeneities in the second subband energy. Point 'O' is a mid-point between the curve extreme points, corresponding to $E_F = E_2$.

holes are captured by the residual ionized acceptors in the $In_{0.53}Ga_{0.47}As$ layer. This leads to a mobility increase as seen in figure 1. Note that the mobility reaches a maximum at $n_s = 3.4 \times 10^{11}$ for sample No 1 and 4.8×10^{11} cm^{-2} for sample No 2. This corresponds to the onset of a new intersubband scattering channel when the Fermi level crosses the bottom of the second subband $E_F > E_2$. For an ideal 2DEG system the density of states is equal to $g_0 = m/\pi\hbar^2$ when $E_F < E_2$ and abruptly increases to $2g_0$ at $E_F = E_2$. This corresponds to a sharp increase in the transport relaxation rate

$$\frac{1}{\tau} = \frac{1}{\tau_1} + \frac{1}{\tau_{12}} \tag{1}$$

($1/\tau_{12}$: intersubband relaxation rate) as shown by the dotted line in figure 1(a). In practice, a smooth variation around the transition energy is seen (experimental points in figure 1) and can be described by a Gaussian broadening caused by the spatial inhomogeneity [21]. This results

in the following density of states near the second subband edge:

$$g_2 = \frac{g_0}{2}\left(1 + \mathrm{erf}\left(\frac{E - E_2}{\sqrt{2}\Gamma_2}\right)\right) \tag{2}$$

where $\mathrm{erf}(x)$ is an error function, E_2 is the mean value of the second subband bottom, and Γ_2 is the mean variation in E_2. Since the probability of intersubband transitions is proportional to the density of states at the Fermi level, equation (1) becomes

$$\frac{1}{\tau} = \frac{1}{\tau_1} + \frac{1}{2\tau_{12}}\left(1 + \mathrm{erf}\left(\frac{e_\mathrm{F}}{\sqrt{2}\Gamma_2}\right)\right) \tag{3}$$

where $e_\mathrm{F} = E_\mathrm{F} - E_2$.

The 2DEG density is thus

$$n_s = g_0(e_\mathrm{F} + E_2) + \frac{g_0}{2}\int_{-\infty}^{\infty}\left(\exp\left(\frac{x - e_\mathrm{F}}{k_\mathrm{B}T}\right) + 1\right)^{-1}\left(1 + \mathrm{erf}\left(\frac{x}{\sqrt{2}\Gamma_2}\right)\right)\mathrm{d}x. \tag{4}$$

The first term in equation (4) is the electron density in the first subband n_1, and the second term corresponds to the electron density in the second subband n_2 when the Fermi level crosses the bottom of the second subband.

The method used to estimate parameters of the density of states and intersubband scattering rate from the experimental dependence $\frac{1}{\tau}(n_s)$ is presented in figure 1(a). The 'mid-point' marked as 'O' between the two extreme points of the curve corresponds to $e_\mathrm{F} = 0$. According to theory, when $k_\mathrm{B}T, \Gamma_2 \ll E_2$ the coordinates of the mid-point are $n_\mathrm{O} \cong g_0 E_2$ and $\frac{1}{\tau_\mathrm{O}} = \frac{1}{\tau_1} + \frac{1}{2\tau_{12}}$. Comparison with the experimental coordinates of the 'mid-point' in figures 1(a) and (b) provides an estimate of E_2 and $\frac{1}{\tau_{12}}$ for our samples. These parameters were used as initial parameters for fitting full experimental $\frac{1}{\tau}(n_s)$ dependences using equations (3) and (4). The first step was to vary the value of Γ_2 to fit the extreme point positions and then best fit curves (solid curves in figure 1) were obtained optimizing values of E_2 and $\frac{1}{\tau_{12}}$ around initial values. The resulting values for the intersubband scattering time τ_{12} and parameters for the second subband energy distribution E_2, Γ_2 are given in table 1.

The influence of spin–orbit interactions on weak localization has been well studied for selectively doped $In_{0.53}Ga_{0.47}As$/InP heterostructures with electrons filling the ground subband only. The first observation of an antilocalization maximum was reported in 1984 [22]. Comprehensive investigations were recently made on a series of samples in the equilibrium state [7, 11] and in the nonequilibrium, persistent photoconductivity, states [12]. Analysis of experiments was based on theory [4] which considers two types of spin–orbit interaction. The first is the Dresselhaus term [23] corresponding to bulk inversion asymmetry (BIA) of the crystal lattice, and the second is the Rashba term [24] concerned with the structural inversion asymmetry (SIA) of the conducting channel in heterostructures. Results obtained over a wide range of 2DEG density permitted the contributions of different spin splitting mechanisms to be separated and showed that structural inversion asymmetry plays the most important role in $In_{0.53}Ga_{0.47}As$/InP structures, especially at high 2DEG densities. Therefore, we can neglect the Dresselhaus term and interference between the BIA and SIA terms. As a result spin coherence can be described by a single parameter:

$$\frac{1}{\tau_s} = \frac{2\tau}{\hbar}\alpha^2 k_\mathrm{F}^2 \tag{5}$$

(α is a SIA constant, k_F is Fermi vector) and the following equation can be used to describe the normalized magnetoconductivity $\Delta\sigma/G_0 \equiv (\sigma(B) - \sigma(0))/(e^2/2\pi^2\hbar)$ for electrons in

the first subband [25, 26]:

$$\frac{\Delta\sigma}{G_0} = f_2\left(\frac{B}{H_\varphi + H_s}\right) + \frac{1}{2} f_2\left(\frac{B}{H_\varphi + 0.5H_s}\right) - \frac{1}{2} f_2\left(\frac{B}{H_\varphi}\right), \tag{6}$$

$$H_i = \frac{\hbar c}{4eD\tau_i}. \tag{7}$$

$f_2(x) = \Psi(\frac{1}{2} + \frac{1}{x}) + \ln(x)$, where $\Psi(x)$ is the digamma function; D is the diffusion coefficient.

To establish an equation for the quantum correction to the conductivity in a two-subband system, we use results from the rigorous theory of weak localization in multilevel quantum wells [13]. Some limiting cases were theoretically studied in [27]. In the most common case intersubband scattering is weak, $\tau \ll \tau_{12}$, because the scattering potential is smooth. The diffusion coefficients D_1 and D_2 can be defined for the electrons in each subband giving the following equation for magnetoconductivity:

$$\frac{\Delta\sigma}{G_0} = \sum_{n=1}^{2}\left[f_2\left(\frac{B}{H_{\mathrm{I}}^{(n)}}\right) + \frac{1}{2} f_2\left(\frac{B}{H_{\mathrm{II}}^{(n)}}\right) - \frac{1}{2} f_2\left(\frac{B}{H_{\mathrm{III}}^{(n)}}\right)\right], \tag{8}$$

where both $H_i^{(1)}$ and $H_i^{(2)}$ are determined by the diffusion coefficients, rates of phase and spin decoherence in the first and second subbands as well as by the rate of intersubband scattering (see [13]). The spin-dependent part of the intersubband transition time is neglected because the spin–orbit interaction is weak and $\tau_{12s} \gg \tau_{12}, \tau_\varphi, \tau_s$. Therefore intersubband transitions play the role of an additional phase breaking mechanism.

If the scattering potential is sharp, then $\tau \sim \tau_{12} \ll \tau_\varphi, \tau_s$ and equation (6) can be used for the magnetoconductivity. An averaged diffusion coefficient derived from the conductivity must be used. Phase and spin breaking rates have to be averaged with weights determined by the density of states in the first (g_1) and second (g_2) subbands:

$$\frac{1}{\tau_i} = \frac{\sum_{n=1}^{2} \frac{g_n}{\tau_i^{(n)}}}{\sum_{n=1}^{2} g_n}. \tag{9}$$

If $\tau \ll \tau_s$ and spin–orbit interaction is weak, then $\tau_{12} \ll \tau_{12s}$. In this case, the rate of spin-dependent intersubband scattering $1/\tau_{12s}$ can be comparable to the rate of spin–orbit intrasubband scattering. Therefore, to get the total spin decoherence rate one must add $1/\tau_{12s}$ to equation (9). One of the tasks of this study was to find clear experimental confirmation for this intersubband mechanism for spin decoherence.

Typical experimental $\frac{\Delta\sigma(B)}{G_0}$ dependences with antilocalized minimum are presented in the inset of figure 2(a) (points). To extract phase and spin coherence parameters we fit the experimental curves using equation (6). In accord with theory the value of $\frac{\Delta\sigma}{G_0}|_{\min}$ is determined by the ratio $\frac{H_\varphi}{H_s}$, only. Therefore, the values and positions of extremes were used to estimate fitting parameters H_φ and H_s. These parameters were just slightly varied to fit the experimental curve at small magnetic field up to $B \approx 0.5H_{\mathrm{tr}}$ (where $H_{\mathrm{tr}} = \frac{\hbar c}{4eD\tau}$). The condition $B < H_{\mathrm{tr}}$ determines the applicability of the diffusion approach, which lies at the basis of weak localization theory. The resulting theoretical curve is presented as a solid line in the inset of figure 2(a). Fitting parameters with uncertainty (error bars) for two samples can be found in figure 2 in the form of the density dependences of H_φ and H_s. Vertical lines in these figures correspond to the minimum transport relaxation rate (see figure 1). Values of characteristic coherence times τ_φ, τ_s calculated from H_φ and H_s at these 2DEG densities are presented in the table 1 as values characterizing the spin and phase coherence of electrons in the first subband. One can see that the presence of electrons in the second subband results in a fast increase of H_φ with a simultaneous slow decrease of H_s. It is important to note that equation (6)

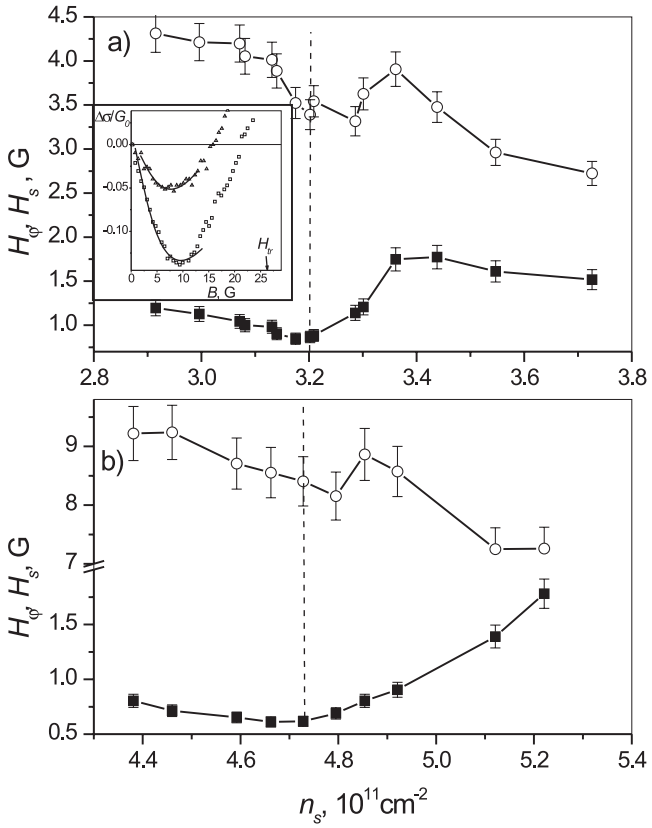

Figure 2. The density dependence of the characteristic magnetic fields for phase H_φ (closed points) and spin decoherence H_s (open points), obtained by fitting the experimental magnetoresistance curves (see the inset) with weak localization theory—equation (6) for samples No 1 (a) and No 2 (b). Vertical dotted lines indicate the 2DEG density corresponding to the minima of the $\tau^{-1}(n_s)$ dependences (see figure 1). Inset: typical experimental dependences of the normalized magnetoconductivity on magnetic fields (points). The line is a result of fitting experimental data in the magnetic fields $B \leqslant 0.5H_{\rm tr}$ providing applicability of the weak localization theory.

can be used to describe the magnetoconductivity of the system with two filled subbands only in the case of fast intersubband scattering $\tau \sim \tau_{12} \ll \tau_\varphi, \tau_s$. As discussed above, we chose samples dominated by short range scattering and providing effective intersubband scattering. As can be seen, sample No 1 fully satisfies this condition. For the second sample, intersubband scattering is faster than phase decoherence but slower than spin decoherence. A quantitative analysis of both samples is given below.

Each point in figure 2 corresponds to a new sample state after a short light pulse, and to a new position of the Fermi level relative to the average second subband edge. Intersubband scattering is sufficiently fast to introduce an averaged diffusion coefficient

$$D = \left(\frac{\sigma}{e^2}\right) \Big/ \left(\frac{{\rm d}n_s}{{\rm d}E_{\rm F}}\right). \tag{10}$$

By differentiating equation (4) the diffusion coefficient was calculated for different 2DEG densities corresponding to the experimental points in figure 2. Using equation (7), we

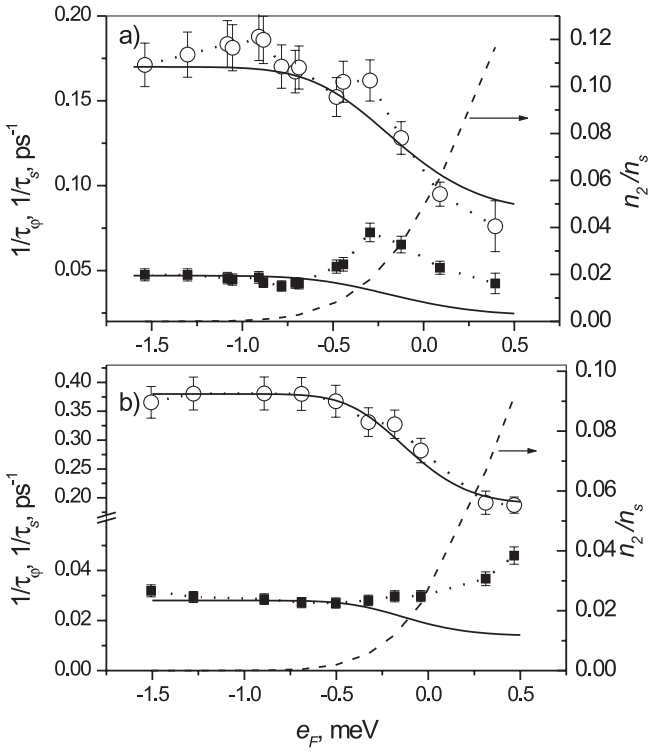

Figure 3. Phase $1/\tau_\varphi$ (closed points) and spin $1/\tau_s$ (open points) decoherence rates versus position of the Fermi level, relative to the averaged value of the second subband bottom $e_{\rm F} = E_{\rm F} - E_2$ for samples No 1 (a) and No 2 (b). The solid curve is calculated using equation (11) suggesting very slow decoherence in the second subband. Dotted curves correspond to right axes and demonstrate the energy dependence of the second subband occupation.

determined the phase $1/\tau_\varphi$ and spin decoherence rates $1/\tau_s$ over the range of 2DEG densities studied. Experimental dependences of these decoherence rates on the Fermi level position $e_{\rm F}$ are given in figure 3 (points) for two samples. Dotted curves in figure 3 show the relative population of the second subband (right axis). When noticeable occupation of the second subband occurs, the decoherence rate changed but in a different manner for phase and spin coherence. The phase decoherence rate increases while the spin decoherence rate decreases. To analyse these dependences we use equation (9) which can be rewritten as follows:

$$\frac{1}{\tau_i} = \frac{\frac{1}{\tau_i^{(1)}} + \frac{1}{\tau_i^{(2)}}\left(\frac{1}{2} + \frac{1}{2}\mathrm{erf}\left(\frac{e_{\rm F}}{\sqrt{2}\Gamma_2}\right)\right)}{\left(\frac{3}{2} + \frac{1}{2}\mathrm{erf}\left(\frac{e_{\rm F}}{\sqrt{2}\Gamma_2}\right)\right)} \tag{11}$$

where i is φ for phase decoherence and s for spin decoherence; the upper index corresponds to the subband number. Under the experimental conditions used, the electron density variation in the first subband is very weak—less than 10%. This allows us to assume that the decoherence rates in the first subband $1/\tau_\varphi^{(1)}$, $1/\tau_s^{(1)}$ are constant. As a first step, we assume that decoherence in the second subband is very slow. The solid curves in figure 3 were obtained from equation (11) with $1/\tau_\varphi^{(2)} = 1/\tau_s^{(2)} = 0$. These calculations can now be compared with the experimental data.

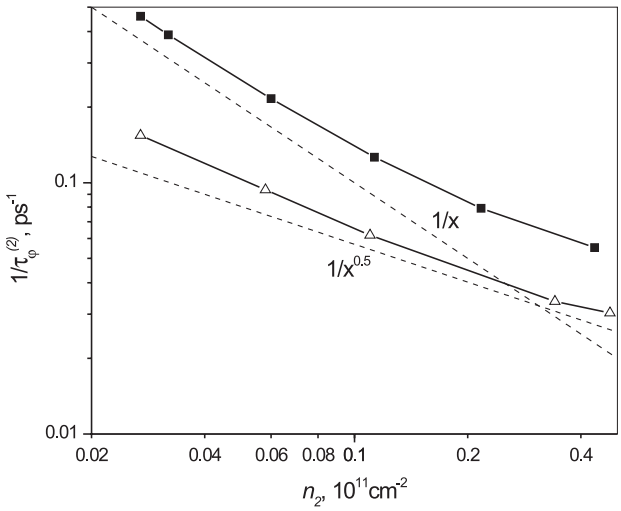

Figure 4. The phase decoherence rate of electrons in the second subband versus electron density in the second subband, for each sample. Closed points—sample No 1, open points—sample No 2. Dotted lines represent $y \sim \frac{1}{x}$ and $\sim \frac{1}{\sqrt{x}}$ proportionalities.

One can see that for both samples, the calculated curves quantitatively describe the experimental dependence for the spin decoherence rate (open symbols in figure 3) for all Fermi level values. This means that spin decoherence in the second subband is much slower than in the first subband and can be neglected. Slow spin relaxation in the second subband can be attributed to a small spin–orbit splitting at small Fermi wavevector for the weakly occupied second subband. According to theory [28], the spin decoherence rate strongly increases with the Fermi wavevector $1/\tau_s \sim (k_\mathrm{F})^p$, where $p > 2$ and

$$\frac{1/\tau_s^{(2)}}{1/\tau_s^{(1)}} \sim \left(\frac{k_\mathrm{F}^{(2)}}{k_\mathrm{F}^{(1)}}\right)^p \sim \left(\frac{n_2}{n_1}\right)^{p/2} < 0.1,$$

which is in good agreement with experimental results. It is clear that any additional scattering channel will increase the calculated values and degrade the agreement between experimental and calculated curves. This means that spin flip intersubband scattering does not play a noticeable role in the spin decoherence of the electrons occupying the two quantum subbands. An estimation of $1/\tau_{12s}$ can be made using data from table 1 suggesting that $\tau_s/\tau = \tau_{12s}/\tau_{12}$. This estimation gives $\frac{1}{\tau_{12s}}/\frac{1}{\tau_s^{(1)}} \sim 0.2$–$0.5$ and predicts a noticeable influence of intersubband spin scattering, which contradicts the experimental results.

Small fluctuations of experimental $1/\tau_s$ are observed in figure 3 (especially for sample No 1) for very weak occupation of the second subband and can be attributed to the influence of electrons localized in the tail of the second subband.

A totally different picture is observed for the phase decoherence rate. When electrons appear in the second subband, the experimental dependence (solid points in figure 3) demonstrates a rise in the decoherence rate while calculations predict a decrease of $1/\tau_\varphi$ (solid curves in figure 3). As a result, the experimental values of the phase decoherence rate noticeably exceed the calculated values. This discrepancy can be attributed to the important role of phase relaxation processes in the second subband. By comparing the experimental data and equation (11) the phase decoherence rate in the second subband, $1/\tau_\varphi^{(2)}$ can be determined. Dependences of $1/\tau_\varphi^{(2)}$ on electron density in the second subband n_2 are presented in figure 4

for the two samples. Comparing figures 3 and 4 it can be seen that the phase decoherence rate in the second subband is far larger than for the first subband. Another important fact is that the phase relaxation rate quickly decreases with increasing electron density in the second subband $1/\tau_{\varphi}^{(2)} \sim (n_2)^{-p}$ where $p = 0.5$–1. We cannot compare results with theoretical prediction for phase breaking due to electron–electron interactions [29, 30] because we cannot decouple electrons in each subband due to the rapid intersubband scattering.

In conclusion, the combination of phase and spin decoherence in a 2DEG was studied. In particular, we focused on electron decoherence involving the second quantum subband for selectively doped InP/$In_{0.53}Ga_{0.47}As$ heterostructures grown by LPE. Short range electron elastic scattering in these structures determined the high rate of the intersubband scattering. Persistent photoconductivity was used to vary the electron density and filling of the second quantum subband. Analysis of $\mu(n_s)$ was made taking into account the density of states variation caused by spatial inhomogeneity. Extracted parameters of inhomogeneity were used to calculate the decoherence rates from characteristic parameters determined by fitting experimental magnetoresistance curves with antilocalization maxima. Theory for fast intersubband scattering and only one mechanism for spin–orbit scattering has been used.

As a result, experimental dependences of the spin and phase decoherence rates on the Fermi level position below and above the second subband edge were determined. By comparing these dependences with theory we showed that (a) there was a negligible role for intersubband transitions in the spin decoherence and slow spin decoherence of electrons in the second quantum subband, attributable to the small value of the in-plane wavevector of electrons in the second subband, and (b) large values of the phase decoherence rate of electrons in the second quantum subband decreasing with second subband population increase. We are currently attempting to develop a theory to explain this result.

References

[1] Wolf S A, Awshalom D D, Buhrman R A, Daughton J M, von Molnar S, Roukes M L, Chtchelkanova A Y and Treger D M 2002 *Science* **294** 1488

[2] Kane B E 1998 *Nature* **393** 133

[3] Averkiev N S and Golub L E 1999 *Phys. Rev.* B **60** 15582

[4] Iordanskii S V, Lyanda-Geller Yu B and Pikus G E 1994 *JETP Lett.* **60** 206

[5] Averkiev N S, Golub L E and Willander M 2002 *J. Phys.: Condens. Matter* **14** R271

[6] Knap W, Skierbiszewski C, Zduniak A, Litwin-Staszewska E, Bertho D, Kobbi F, Robert J L, Pikus G E, Pikus F G, Iordanskii S V, Mosser V, Zekentes K and Lyanda-Geller Yu B 1996 *Phys. Rev.* B **53** 3912

[7] Kreshchuk A M, Novikov S V, Polyanskaya T A and Savel'ev I G 1997 *Semiconductors* **31** 391

[8] Altshuler B L and Aronov A G 1985 *Modern Problems in Condensed Matter Sciences* vol 10, ed A L Efros and M Pollak (Amsterdam: North-Holland)

[9] Hikami S, Larkin A I and Nagaoka Y 1980 *Prog. Theor. Phys.* **44** 707

[10] Dresselhaus P D, Papavassiliou C M A, Wheeler R G and Sacks R N 1992 *Phys. Rev. Lett.* **68** 106

[11] Kreshchuk A M, Novikov S V, Polyanskaya T A and Savel'ev I G 1998 *Semicond. Sci. Technol.* **13** 384

[12] Bikanov D D, Novikov S V, Polyanskaya T A and Savel'ev I G 2002 *Semiconductors* **36** 1389

[13] Averkiev N S, Golub L E and Pikus G E 1998 *Semiconductors* **32** 1087

[14] Lee K, Shur M S, Drummond T J and Morkoç H 1983 *J. Appl. Phys.* **54** 6432

[15] Golubev L V, Kreshchuk A M, Novikov S V, Polyanskaya T A, Savel'ev I G and Saidashev I I 1988 *Sov. Phys.—Semicond.* **22** 1234

[16] Vorob'eva V V, Egorova M V, Kreshchuk A M, Novikov S V and Savel'ev I G 1989 *Sov. Phys.—Semicond.* **23** 1051

[17] Kreshchuk A M, Novikov S V and Savel'ev I G 1992 *Sov. Phys.—Semicond.* **26** 771

[18] Kreshchuk A M, Novikov S V, Polyanskaya T A, Savel'ev I G and Shik A Ya 1995 *J. Cryst. Growth* **146** 153

[19] Walukievicz W, Ruda H E, Lagovski J and Gatos H C 1984 *Phys. Rev.* B **30** 4571

[20] Guillemot C, Baudet M, Gaueau M and Regreny A 1987 *Phys. Rev.* B **35** 2799

[21] Shklovskii B I and Efros A L 1984 *Electronic Properties of Doped Semiconductors* (Berlin: Springer)

[22] Alferov Zh I, Gorelenok A T, Mamutin V V, Polyanskaya T A, Savel'ev I G and Shmartsev Yu V 1984 *Sov. Phys.—Semicond.* **18** 1247
[23] Dresselhaus G 1955 *Phys. Rev.* **100** 580
[24] Bychkov Yu L and Rashba E I 1984 *J. Phys. C: Solid State Phys.* **17** 6093
[25] Abrahams E, Anderson P W, Licciardello D C and Ramakrishnan T V 1979 *Phys. Rev. Lett.* **42** 673
[26] Altshuler B L and Aronov A G 1979 *Sov. Phys.—JETP* **50** 968
[27] Iwabuchi Sh and Nagaoka Y 1989 *J. Phys. Soc. Japan* **50** 1325
[28] Golub L E, Averkiev N S and Willander M 2000 *Nanotechnology* **11** 215
[29] Altshuler B L, Aronov A G and Khmelnitsky D E 1982 *J. Phys. C: Solid State Phys.* **15** 7367
[30] Fukuyama H and Abrahams E 1983 *Phys. Rev.* B **27** 5976